Hindawi Publishing Corporation
Journal of Chemistry
Volume 2016, Article ID 2418172, 10 pages
http://dx.doi.org/10.1155/2016/2418172

Research Article

Fe_3O_4/Reduced Graphene Oxide Nanocomposite: Synthesis and Its Application for Toxic Metal Ion Removal

Nguyen Thi Vuong Hoan,[1] Nguyen Thi Anh Thu,[2] Hoang Van Duc,[2] Nguyen Duc Cuong,[3] Dinh Quang Khieu,[4] and Vien Vo[1]

[1]*Quy Nhon University, 170 An Duong Vuong, Quy Nhon City, Vietnam*
[2]*College of Pedagogy, Hue University, 34 Le Loi, Hue City, Vietnam*
[3]*Faculty of Hospitality and Tourism, Hue University, 22 Lam Hoang, Hue City, Vietnam*
[4]*College of Science, Hue University, 77 Nguyen Hue, Hue City, Vietnam*

Correspondence should be addressed to Nguyen Thi Vuong Hoan; nguyenthivuonghoan@qnu.edu.vn
and Vien Vo; vovien@qnu.edu.vn

Received 16 March 2016; Revised 8 August 2016; Accepted 23 August 2016

Academic Editor: Carola Esposito Corcione

The synthesis of reduced graphene oxide modified by magnetic iron oxide (Fe_3O_4/rGO) and its application for heavy metals removal were demonstrated. The obtained samples were characterized by X-ray diffraction (XRD), nitrogen adsorption/desorption isotherms, X-ray photoelectron spectroscopy (XPS), Fourier transform infrared spectroscopy (FT-IR), and magnetic measurement. The results showed that the obtained graphene oxide (GO) contains a small part of initial graphite as well as reduced oxide graphene. GO exhibits very high surface area in comparison with initial graphite. The morphology of Fe_3O_4/rGO consists of very fine spherical iron nanooxide particles in nanoscale. The formal kinetics and adsorption isotherms of As(V), Ni(II), and Pb(II) over obtained Fe_3O_4/rGO have been investigated. Fe_3O_4/rGO exhibits excellent heavy metal ions adsorption indicating that it is a potential adsorbent for water sources contaminated by heavy metals.

1. Introduction

The content of heavy metals in supplied water has steadily increased over the last years as a result of overpopulation and industrialization. Heavy metals are a well-known highly toxic and carcinogenic element. Its contamination in aqueous system has been a serious concern throughout the world. Arsenic (As), one of the trace elements in drinking water, is toxic to living organism when its concentration exceeds 10 μg/L [1, 2]. Arsenic is introduced into aquatic environment from both natural and man-made sources. Typically, arsenic occurrence in groundwater is caused by the weathering and dissolution of arsenic-bearing rocks, minerals, and ores [3]. Besides, nickel is a nutritionally essential trace metal for at least several animal species, microorganisms, and plants, and therefore either deficiency or toxicity symptoms can occur when too little or too much nickel is taken up. Nickel is an important metal, heavily utilized in industry mainly due to its anticorrosion properties. As a consequence, nickel containing wastes such as spent batteries and catalysts, wastewater, and bleed-off electrolytes are generated in various processes. The environment is polluted by nickel through water, air, and soil and food can be containing it [4, 5]. In addition, pollution of water and soil by lead has been recognized as a serious threat to human health. Pb(II) is known to damage kidney, liver, reproductive system, basic cellular processes, brain functions, and so forth. Waste from metallurgy, electroplating, storage battery, paint, electronics, petroleum refining industry, and so forth released into water bodies is a major source of Pb(II) pollution [6].

A number of techniques including ion exchange [4], floatation [5], and adsorption [1, 2] are prevalent for removal of heavy metal ions from aqueous solutions. As an efficient separation technique, adsorption has been in use for a long time to remove heavy metal ions. Large-scale wastewater treatment systems are employing it now as a cost effective

technique [7]. Numerous materials from natural ones to the specially designed have already been proposed for the adsorption of heavy metals from water [8]. However, such adsorbents can suffer from low adsorption capacities and separation inconveniences. Therefore, the exploration of new promising adsorbents is still desirable.

Graphene and reduced graphene oxide (rGO) are kinds of novel and interesting carbon materials and have attracted tremendous attentions from both the experimental and theoretical scientific communities in recent years [9, 10]. In addition to being the principle component of the most carbon-based nanomaterials, rGO also exhibits extraordinary properties, such as excellent mechanical, electrical, thermal, and very high specific surface area, and it might be also a good candidate as an adsorbent. Recently, graphene-based composites have been applied for the extraction of polycyclic aromatic hydrocarbons [11] and parathyroid pesticides [12] with excellent results. However, to separate the adsorbent of graphene-based composites from the aqueous solution, high-speed centrifugation was needed. Magnetic separation has been one of the promising techniques for environmental water purification because no contaminants such as flocculants and the capability of treating large amount of wastewater within a short time can be obtained [13].

In the past few years, magnetic separation technology has been widely used in the fields of separations and adsorptions [13, 14]. The introduction of magnetic properties into graphene or rGO will combine their high adsorption capacity and the separation convenience of the magnetic materials. The preparations of graphene-based magnetic nanocomposites and their application arsenic removal have been reported recently [15–19]. However, the applications of graphene-based magnetic nanoparticles as the adsorbents for the extraction of Pb(II) and Ni(II) are still very few in the literatures [20–23]. In this work, magnetic reduced graphene oxide nanocomposite (Fe_3O_4/rGO) has been synthesized by a solvothermal method, in which, in addition to providing the magnetic property, Fe_3O_4 can exhibit adsorption sites. The practical application potential for this material in the removal of arsenate, nickel, and lead from aqueous solution has been investigated.

2. Experimental

2.1. Materials. Graphite powder, potassium permanganate ($KMnO_4$), iron(III) chloride hexahydrate ($FeCl_3{\cdot}6H_2O$), iron(II) sulfate heptahydrate ($FeSO_4{\cdot}7H_2O$), sodium nitrate ($NaNO_3$), sodium monohydrogen arsenate ($Na_2HAsO_4{\cdot}2H_2O$), and ethanol (C_2H_5OH) were purchased from Merck. Sulfuric acid (H_2SO_4), hydrogen peroxide (H_2O_2, 30%), ammonia solution (NH_4OH, 25%), hydrochloric acid (HCl), lead nitrate ($Pb(NO_3)_2$), and nickel nitrate ($Ni(NO_3)_2$) were purchased from Sigma-Aldrich. All chemicals are of analytical grade.

2.2. Preparation of GO, rGO, and Fe_3O_4/rGO. The preparation of graphene oxide (GO) was carried out by a modified Hummer's method [24]. In a typical synthesis, 1.0 g of graphite powder was added into 2.5 g of $NaNO_3$ and 100 mL of concentrated H_2SO_4 under stirring. Then 3.0 g of $KMnO_4$ was added gradually to this mixture at 10°C under stirring for 2 h. The resulting mixture was added to 100 mL of distilled water and then heated to 98°C. The obtained mixture was continued to be stirred for 2 h. After that, 10 mL of H_2O_2 was added in the mixture with stirring for 2 h. The color of the mixture changed to bright yellow. Finally, the mixture was filtered and washed with a 5% HCl aqueous solution to remove metal ions, followed by distilled water for removal of the acid. The resulting solid with brown black color was separated by ultrasonic treatment in water and dried at 60°C for 12 h.

To prepare reduced graphene oxide (rGO), as-prepared GO (1.0 g) was ultrasonically dispersed into 300 mL of distilled water in a flask for 1 h under nitrogen atmosphere. The temperature of mixture was then elevated to 80°C, and 10 g of ascorbic acid was added under gradual stirring for 20 minutes. A brown solid was obtained by filtering and washing with ethanol and dried at 80°C in vacuum condition for 10 h.

The Fe_3O_4/rGO nanocomposite, in which the rGO was anchored by Fe_3O_4 nanoparticles, was prepared by a direct method according to the reports [25, 26]. In a typical procedure, rGO (500 mg) was dispersed in distilled water under ultrasonication for 2 h, and then a mixture of $FeSO_4{\cdot}7H_2O$ (0.002 mol) and $FeCl_3{\cdot}6H_2O$ (0.004 mol) was added under ultrasonication for 1 h. A solution of NH_4OH (1.65 M) was taken in dropping under vigorous stirring for 2 h. The obtained black solid was filtered and washed with water and then with ethanol several times to remove residue acid and dissociative Fe(II). The solid was soaked in anhydrous ethanol for 60 min, filtered, and then dried in vacuum at 333 K.

2.3. Characterization of Materials. X-ray diffraction (XRD) analysis was carried out on a D8 Advanced Bruker anode X-ray Diffractometer with Cu Kα (λ = 1.5406 Å) radiation. Transmission electron microscope (TEM) images were obtained by JEOL JEM-2100F. Infrared (IR) spectra for the samples were recorded on an IRPrestige-21 spectrophotometer (Shimadzu). X-ray photoelectron spectrometry (XPS) was conducted by ESCALAB 250. The magnetic property was analyzed using a vibrating sample magnetometer (VSM, MicroSence Easy VSM 20130321-02) at room temperature. Nitrogen physisorption measurements were conducted using a Micromeritics ASAP 2020 analyzer. Samples were pretreated by heating under vacuum at 130°C for 10 h. Specific surface area values of samples were calculated by the Brunauer-Emmett-Teller (BET) method. Metal ions were determined on a Perkin Elmer 3110 spectrometer.

The point of zero charge (pH_{PZC}) of Fe_3O_4/rGO was evaluated by the solid method [27]. According to that, a series of 0.1 M KNO_3 solutions (25 mL) in 250 mL conical flasks was prepared. The initial pH value (pH_i) of the solution was adjusted from 2 to 10 by adding either 0.1 M HCl or 0.1 M NaOH. Then, 0.05 g of Fe_3O_4/rGO was added to each flask and mixtures were agitated. After 24 h, the final pH (pH_f) of solution was measured. The pH variation between the initial solution and final solution ($\Delta pH = pH_i - pH_f$)

was plotted against the pH_i. The point of intersection of curve with abscissa, at which $\Delta pH = 0$, provided pH_{PZC}.

2.4. Adsorption Experiments

2.4.1. Equilibrium Experiments. The equilibrium adsorption of As(V), Pb(II), and Ni(II) on Fe_3O_4/rGO was carried out at various metal ion concentrations and pH values with a constant temperature of 25°C. In this experiment, 250 mL of solution of the metal ion was taken in 500 mL conical flask and the initial pH was adjusted to 5.5–6 for As(V) and Pb(II) and 4.7–5.2 for Ni(II) using HCl or NaOH solutions. 0.1 g of Fe_3O_4/rGO was then added to one of the seven flasks and kept in the shaking incubator for 24 h to ensure equilibrium adsorption at the 25°C. The flask was kept sealed to minimize metal ion concentration change due to water evaporation. The solution was analyzed for metal ion concentration at the equilibrium time, C_e, by AAS. The amount of metal ion adsorbed on the adsorbent at equilibrium time, q_e, was calculated as follows:

$$q_e = \frac{V\left(C_o - C_e\right)}{m}, \quad (1)$$

where C_o is the initial concentration (mg/L) of metal ion, C_e is the concentrations (mg/L) of metal in solution after the adsorption, V is the volume of solution (mL), and m is the weight (g) of Fe_3O_4/rGO.

2.4.2. Effect of pH on As(V), Ni(II), and Pb(II) Adsorption. To investigate pH effect, a series of 50 mL (50 mg/L) of metal ions was put in flasks. The pH of solution was carefully adjusted to the range 2.2–12.4 for As(V) solution and 2–7 for the other metals by adding a small amount of dilute HCl or NaOH solution using a pH meter. Then 0.1 g of Fe_3O_4/rGO was put into each flask and the mixtures were shaken for 24 h. The ion metal concentration of solutions was measured before and after adsorption by AAS. The capacity of adsorbed metal ion is calculated using (1).

2.4.3. Adsorption Kinetics and Isotherms. Kinetics study was conducted by varying initial concentration of the metal ions (As(V), Pb(II), and Ni(II)). 100 mL of metal ion solution with pH 5.5–6 for As(V) and Pb(II) and 4.7–5.2 for Ni(II) was taken into a 500 mL conical flask that was placed in a thermostatically controlled water bath at 25°C with stirring. 0.1 g of Fe_3O_4/rGO was added to the flask. During the experiment, small samples of the mixtures were taken out for analysis at predetermined intervals and then were centrifuged for 10 min to separate the supernatant and the adsorbent. The metal ion concentration, C_t, in the clear supernatant at different time intervals was then determined by AAS. The initial concentration of metal ion C_o was varied from around 20.00 to 100.00 mg/L for As(V), 11.69 to 51.12 mg/L for Ni(II), and 13.10 to 75.80 mg/L for Pb(II).

3. Results and Discussion

3.1. Characterization of Materials. XRD measurements were employed to investigate crystalline phase and structure of the synthesized samples. Figure 1 shows the XRD patterns of GO, rGO, and Fe_3O_4/rGO. The peak at around 11.4° of GO was observed, which is attributed to the introduction of oxygen-containing functional groups into the graphite sheets in the formation of GO [18, 19]. However, broad peaks at around 26°, which can be ascribed to the natural graphite, show the incomplete oxidation of graphite. In fact, the similar results are also obtained in the reported papers [19, 28]. After the reduction with ascorbic acid, the peak at 11.4° disappeared and the weak and broad reflection peak at 25.8° corresponding to the relative short-range order structures in disordered stacked rGO arose [29], which indicates the successful reduction of GO. Figure 1 also shows the XRD pattern of the Fe_3O_4/rGO nanocomposites. The characteristic diffractions of iron oxide match the face-centered cubic crystal Fe_3O_4 (JCPDS file card number 19-0629) implying the existence of magnetic oxide.

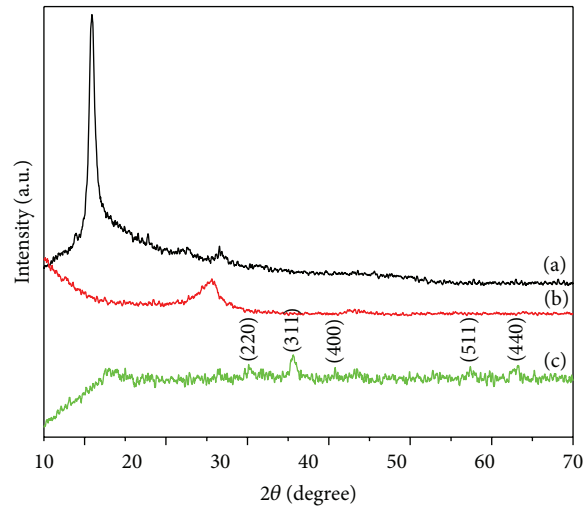

Figure 1: XRD patterns of GO (a), rGO (b), and Fe_3O_4/rGO (c).

The morphologies of GO and Fe_3O_4/rGO were observed as shown in Figure 2. The TEM image of GO shows a stacked and crumpled morphology, revealing deformation because of the exfoliation and restacking process [29] (Figure 2(a)). The Fe_3O_4 particles with average size of 20 nm dispersed well over the rGO sheet were observed (Figure 2(b)). However, it is difficult to obtain monodisperse Fe_3O_4 particles due to their inherent magnetism.

FT-IR spectra of GO, rGO, and Fe_3O_4/rGO are shown in Figure 3. Upon oxidation of graphite to GO, the characteristic peaks of the presence of oxygen in carbon frameworks which include the band at 1730 cm^{-1} (C=O stretching of carbonyl and carboxyl groups), 1412 cm^{-1} (tertiary C-OH groups stretching), and 1060 cm^{-1} (C-O stretching vibration of epoxide) were observed. However, all these absorption bands related to oxidized groups disappear in the FT-IR spectrum of rGO, indicating the reduction of the groups containing oxygen by ascorbic acid. The FT-IR spectrum of Fe_3O_4/rGO differed from that of GO as evidenced by the weakening of the peaks of C=O and 1730 and 3430 cm^{-1},

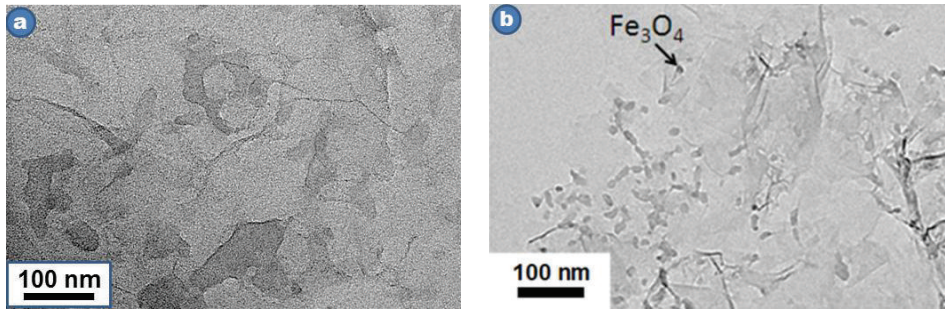

(a) (b)

Figure 2: TEM image of GO (a) and Fe_3O_4/rGO (b).

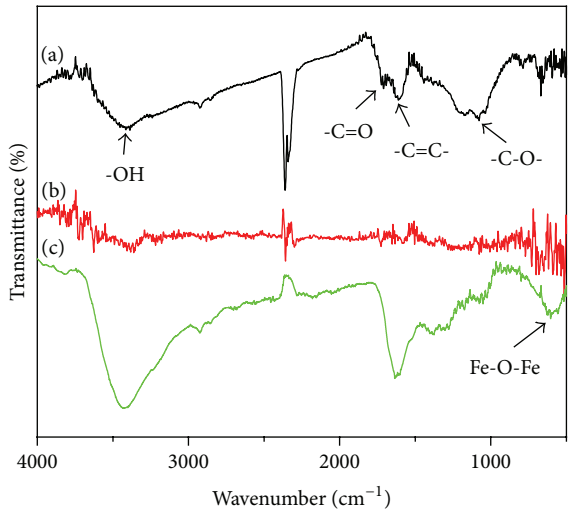

Figure 3: FT-IR spectra of GO (a), rGO (b), and Fe_3O_4/rGO (c).

respectively. The band around 578 cm^{-1} was attributed to Fe-O, replying the existence of Fe_3O_4 [30].

The XPS spectrum in Figure 4(a) shows the wide spectrum of Fe_3O_4/rGO nanocomposite which indicates the presence of the three elements at 285, 530, and 710 eV corresponding to carbon (C 1s), oxygen (O 1s), and Fe 2p, respectively. The high-resolution XPS for C 1s of GO and rGO is shown in Figures 4(b) and 4(c), respectively. The deconvoluted C 1s spectrum demonstrates that GO consists of functional groups including sp^2 (C=C, 284.8 eV), hydroxyl and epoxy (C-O, 286.8 eV), carbonyl (C=O, 287.9 eV), and carboxylates (O=C-O, 288.8 eV) [19]. The high-resolution XPS of C 1s for rGO shows that the intensity of functional groups of rGO remarkably reduced compared with those of GO, indicating an efficient deoxidization. Since XRD patterns of magnetite Fe_3O_4 and maghemite Fe_2O_3 are very similar, XPS Fe 2p core level can be conducted to confirm magnetite. Figure 4(d) shows XPS Fe 2p core level of Fe_3O_4/rGO. It can be seen that characteristic peaks around 719 eV for maghemite are absent, while the broad peaks around 710,9 and 724,5 eV for magnetite are present. This reflects a successful loading of Fe_3O_4 [19].

The VSM magnetic characterization of Fe_3O_4/rGO was determined at room temperature, where the magnetization hysteresis loops appear S-like, and saturation magnetization is 59.4 emu as shown in Figure 5. This value is rather lower than the value of the pure nanomagnetic Fe_3O_4 [30] but higher than those of Fe_3O_4/rGO in the reports [31, 32]. This low saturation magnetization value of Fe_3O_4/rGO in comparison with pure magnetic Fe_3O_4 may be attributed to the presence of reduced graphene oxide nanosheets and the relatively lower density of magnetic components in the nanocomposites. The magnetic coercivity was nearly zero, evidencing no remaining magnetization upon removal of the external magnetic field. Therefore, superparamagnetic behavior of nanocomposites Fe_3O_4/rGO was established.

The nitrogen adsorption/desorption isotherms of the obtained samples corresponding to typical type IV are shown in Figure 6. The presence of hysteresis loop at highly relative pressure region indicates that the mesopore may be formed from the void between the primary particles. The specific surface areas of GO, rGO, and Fe_3O_4/rGO are 318 m^2/g, 386 m^2/g, and 109 m^2/g, respectively. Two reasons for the surface area reduction of Fe_3O_4/rGO can be considered. First, some micropores of rGO were occupied by Fe_3O_4 particles during the synthesis. Second, some parts of the composite powders of Fe_3O_4/rGO were aggregated after Fe_3O_4 particles were incorporated to the composite. All the above data demonstrate that the Fe_3O_4/rGO can be successfully achieved by a simple approach. The formation mechanism of the nanocomposite can be explained as follows [33]:

$$C_6H_8O_6 + GO \longrightarrow rGO + C_6H_6O_6 + 2H^+ \quad (2)$$

$$Fe^{2+} + 2Fe^{3+} + 8OH^- + rGO \longrightarrow Fe_3O_4/rGO + 4H_2O \quad (3)$$

3.2. Adsorption Test. The point of zero charge for Fe_3O_4/rGO determined by solid addition method is around 6.3. It is well known that solution pH plays a significant influence on the adsorption process because it can affect the degree of ionization of pollutants as well as the ionic state of the functional groups on the surface of adsorbent [34]. To investigate the effect of pH on toxic metal ions adsorption, the solution pH was adjusted with HCl and NaOH solutions.

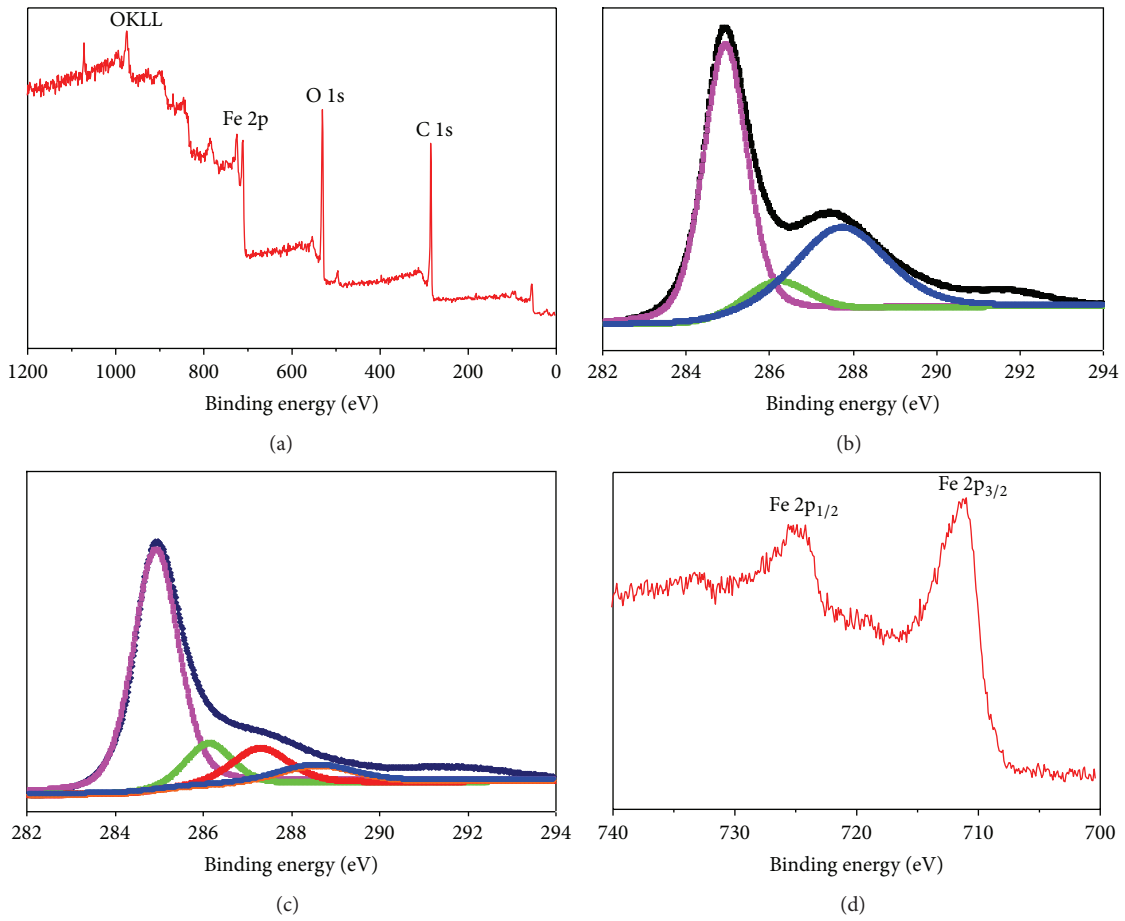

Figure 4: XPS spectrum of Fe_3O_4/rGO (a), XPS C 1s core level spectrum of GO (b), XPS C 1s core level spectrum of rGO (c), and XPS Fe 2p core level spectrum of Fe_3O_4/rGO (d).

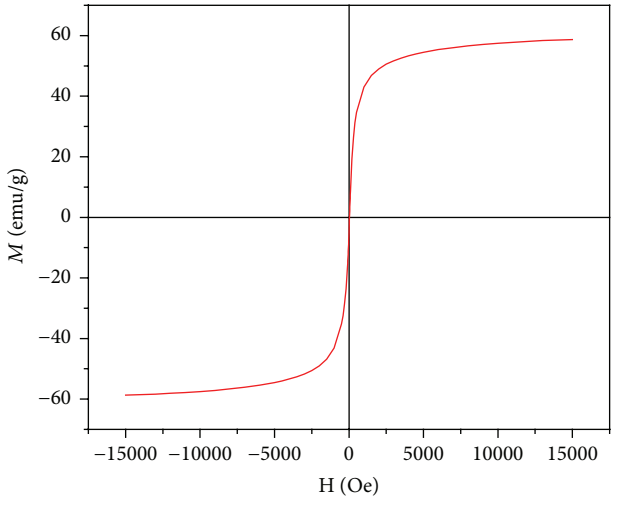

Figure 5: Magnetization curve of Fe_3O_4/rGO.

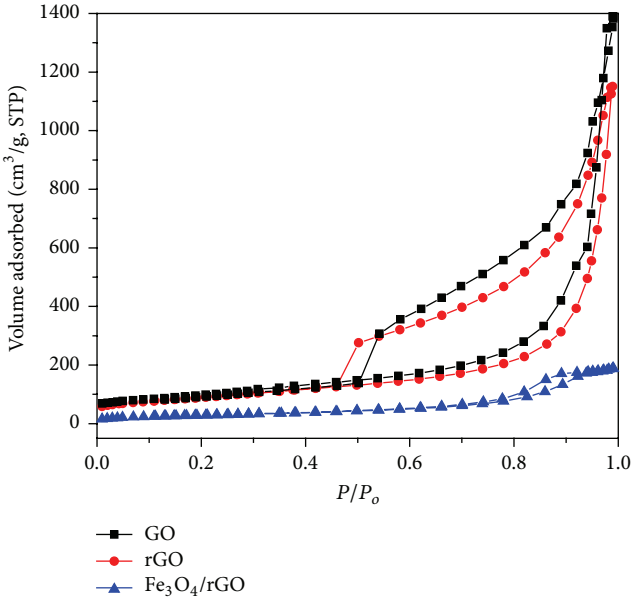

Figure 6: Nitrogen adsorption/desorption isotherms of GO, rGO, and Fe_3O_4/rGO.

To avoid precipitation of lead (II) and nickel (II) hydroxides, the experiments were performed in the pH range from around 2.0 to 7.0, whereas the solution pH for adsorption of As(V) was used at the range of 2.0–12.0. As shown in Figure 7, the adsorption amount of As(V), Ni(II), and Pb(II) increased with an increase of pH from 2 to 6.27, 5.02, and 5.65, respectively, while it decreased with a further

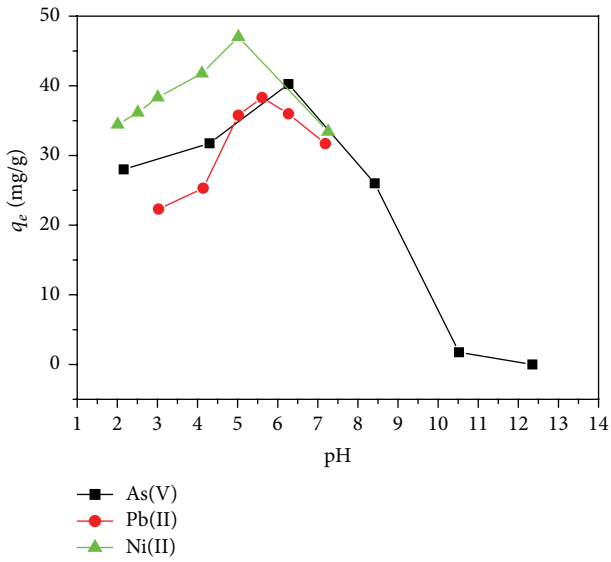

FIGURE 7: Influence of pH on the adsorption of As(V), Pb(II), and Ni(II).

increased pH. This phenomenon can be explained by two effects: (i) Protonation under acidic condition or ionization under neutral and basic conditions for the surface hydroxyl functional groups of Fe_3O_4/rGO can take place, following (4) and (5) [35]; (ii) the electrostatic repulsion between metal species and charges of the sorbent surface would also lead to a decrease in the removal extent of metal ions at stronger acidic conditions and pH > pH_{PZC} [36].

Protonation Process

$$(Fe_3O_4/rGO)\text{-}OH + H^+ \rightleftarrows (Fe_3O_4/rGO)\text{-}OH_2^+ \quad (4)$$

Ionization Process

$$(Fe_3O_4/rGO)\text{-}OH \rightleftarrows (Fe_3O_4/rGO)\text{-}O^- + H^+ \quad (5)$$

Figure 8 shows the adsorption data of different concentrations for As(V), Ni(II), and Pb(V) with time. It can be seen that the adsorption capacity of Fe_3O_4/rGO for As(V) increases with the initial As(V) concentration from 13.1 ppm to 75.8 ppm. This observation can be attributed to the enhanced interaction between the arsenate and adsorbent with accreting initial As(V) concentration [37]. Moreover, the mass transfer driving force becoming larger as an increase of the initial concentration is attributed to higher uptake of As(V) from aqueous solution [38]. The process shows a very fast adsorption rate, which can be verified by the fact that the amount of adsorbed As(V) on Fe_3O_4/rGO composite in As(V) solution is around 60% within 25 minutes. The time required to reach the adsorption equilibrium between the Fe_3O_4/rGO and As(V) in the solution was less than 170 min. The similar trends occurred in the cases of Ni(II) and Pb(II) adsorption (Figures 8(b) and 8(c)).

The *pseudo*-first-order and *pseudo*-second-order kinetic models were used to investigate the kinetics of metal adsorption on the Fe_3O_4/rGO composite. The *pseudo*-first-order model in linear form could be expressed [39] as

$$\ln(q_e - q_t) = \ln q_e - k_1 t, \quad (6)$$

where q_e and q_t are the amounts of metal ion adsorbed on adsorbent (mg·g^{-1}) at equilibrium and at time t, respectively, and k_1 is the rate constant of first-order adsorption (min^{-1}). Straight-line plots of $\ln(q_e - q_t)$ against t were used to determine the rate constant, k_1.

The *pseudo*-second-order model in linear form may be expressed as [40]

$$\frac{t}{q_t} = \frac{1}{(k_2 q_e^2)} + \frac{t}{q_e}, \quad (7)$$

where k_2 is the rate constant of second-order adsorption (g mg^{-1} min^{-1}). Straight-line plots of t/q_t against t were tested to obtain rate parameters.

A comparison of *pseudo*-first-order and pseudo-second-order kinetic models of metal adsorption onto Fe_3O_4/rGO at various initial concentrations is illustrated in Tables 1, 2, and 3. The results show that the coefficients of determination (R^2) for *pseudo*-second-order model are higher compared with those of *pseudo*-first-order one and the calculated q_e values ($q_{e,cal}$) from this model agree well with the experimental data ($q_{e,exp}$). These results suggest that the kinetics of As(V), Ni(II), or Pb(II) adsorption on the Fe_3O_4/rGO follow the *pseudo*-second-order model.

The adsorption isotherm models of Langmuir and Freundlich were applied to fit the adsorption equilibrium data of As(V), Ni(II), and Pb(II) on Fe_3O_4/rGO composite. According to the Langmuir isotherm model, adsorption takes place at specific homogeneous sites on a sorbent and the linear form can be written as [41]

$$\frac{C_e}{q_e} = \frac{1}{(K_L q_m)} + \frac{C_e}{q_m}, \quad (8)$$

where q_e and C_e are the equilibrium metal ion contents on the sorbent (mg g^{-1}) and in the solution (mg L^{-1}), respectively, q_m is the maximum monolayer adsorption capacity of the sorbent (mg g^{-1}), and K_L is the Langmuir adsorption constant (L mg^{-1}).

Freundlich isotherm model assumes a heterogeneous adsorption surface and active sites with different energy, and the Freundlich isotherm model is given in linear form as [42]

$$\ln q_e = \ln K_F + \left(\frac{1}{n}\right) \ln C_e, \quad (9)$$

where K_F (mg g^{-1}) is the Freundlich constant, which is a measure of adsorption capacity, and $1/n$ is an empirical parameter related to the nature and strength of the adsorption process and the distribution of the active sites. Low values of $1/n$ mean that the surface is heterogeneous. For values in the range $0.1 < 1/n < 1$, adsorption is favorable [37]. The Langmuir and Freundlich isotherm parameters for metal ion

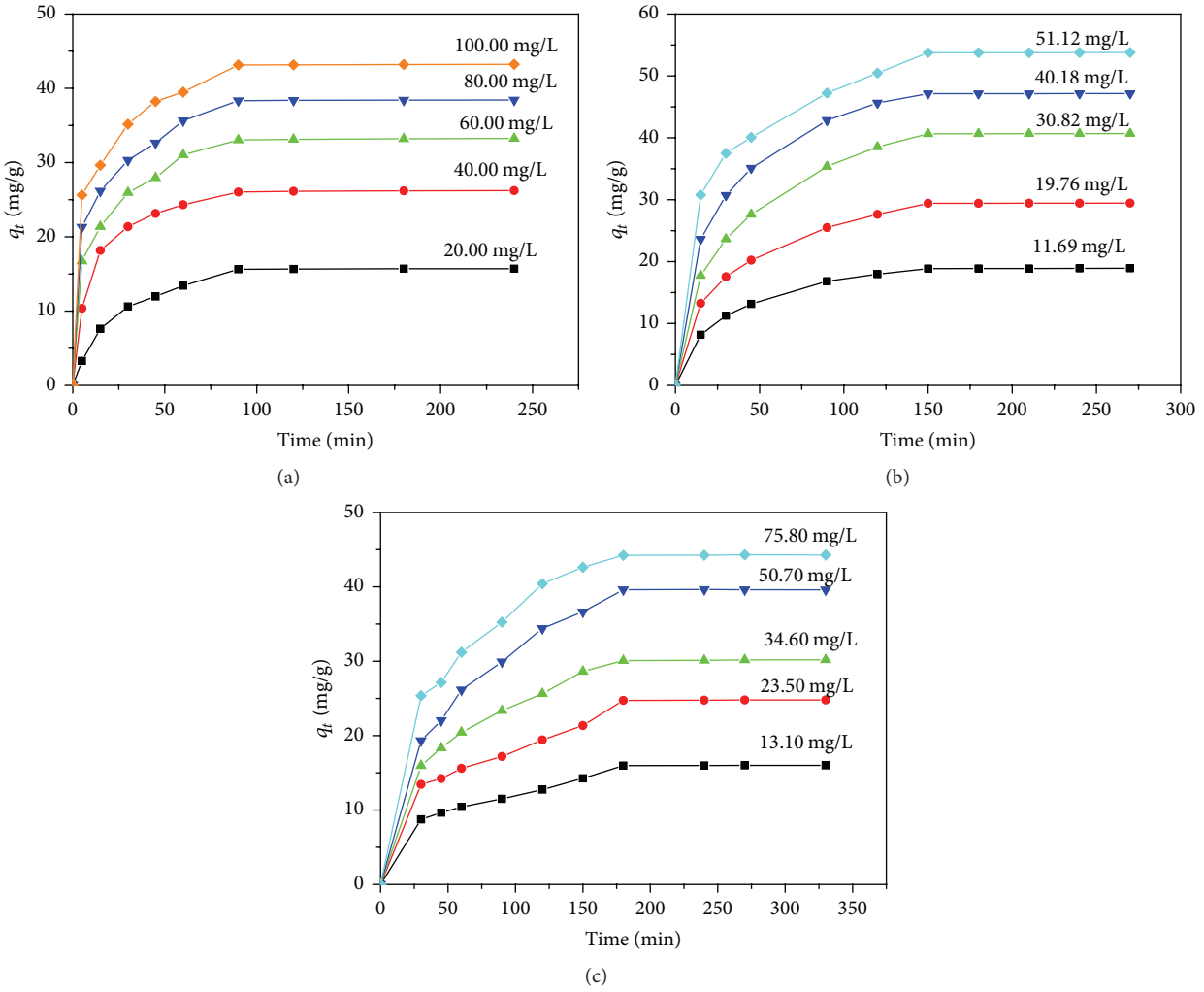

Figure 8: Adsorption kinetics of As(V) (a), Ni(II) (b), and Pb(II) (c) over Fe_3O_4/rGO with different concentrations.

Table 1: Adsorption kinetic parameters for As(V) adsorption on the Fe_3O_4/rGO composite.

C_o (mgL^{-1})	*Pseudo*-first-order kinetics			*Pseudo*-second-order kinetics			
	k_1 (min^{-1})	$q_{e,cal}$ ($mg{\cdot}g^{-1}$)	R^2	k_2 ($g{\cdot}mg^{-1}{\cdot}min^{-1}$)	$q_{e,cal}$ ($mg{\cdot}g^{-1}$)	$q_{e,exp}$ ($mg{\cdot}g^{-1}$)	R^2
13.10	0.0112	10.84	0.9539	0.0017	16.77	15.97	0.9841
23.50	0.0099	16.36	0.9706	0.0011	25.28	24.40	0.9831
34.60	0.0156	21.07	0.8969	0.0011	32.65	30.90	0.9866
50.70	0.0160	35.56	0.9883	0.0008	43.29	39.61	0.9936
75.80	0.0206	42.77	0.9639	0.0005	53.30	44.23	0.9896

Table 2: Adsorption kinetic parameters for Ni(II) adsorption on the Fe_3O_4/rGO composite.

C_o (mgL^{-1})	*Pseudo*-first-order kinetics			*Pseudo*-second-order kinetics			
	k_1 (min^{-1})	$q_{e,cal}$ ($mg{\cdot}g^{-1}$)	R^2	k_2 ($g{\cdot}mg^{-1}{\cdot}min^{-1}$)	$q_{e,cal}$ ($mg{\cdot}g^{-1}$)	$q_{e,exp}$ ($mg{\cdot}g^{-1}$)	R^2
11.69	0.0228	15.50	0.9982	0.0015	22.37	18.88	0.9988
19.78	0.0204	22.47	0.9948	0.0010	34.36	29.41	0.9966
30.82	0.0220	33.62	0.9907	0.0007	48.31	40.65	0.9970
40.18	0.0254	36.22	0.9906	0.0009	53.76	47.12	0.9990
51.11	0.0177	29.61	0.9930	0.0010	58.48	53.75	0.9956

Table 3: Adsorption kinetic parameters for Pb(II) adsorption on the Fe_3O_4/rGO composite.

C_o (mgL^{-1})	*Pseudo*-first-order kinetics			*Pseudo*-second-order kinetics			
	k_1 (min^{-1})	$q_{e,\text{cal}}$ (mg·g^{-1})	R^2	k_2 (g·mg^{-1}·min^{-1})	$q_{e,\text{cal}}$ (mg·g^{-1})	$q_{e,\text{exp}}$ (mg·g^{-1})	R^2
20.00	0.0300	13.31	0.9896	0.0025	18.15	15.63	0.9976
40.00	0.0385	16.15	0.9805	0.0044	27.52	26.03	0.9997
60.00	0.0360	20.51	0.9691	0.0040	33.70	33.03	0.9910
80.00	0.0318	20.39	0.9805	0.0044	37.98	38.33	0.9932
100.00	0.0296	20.13	0.9914	0.0047	42.34	43.14	0.9966

Table 4: Adsorption isotherm parameters for metal adsorption on Fe_3O_4/rGO composite.

Ions	Langmuir isotherm			Freundlich isotherm		
	K_L (L·mg^{-1})	q_m (mg·g^{-1})	R^2	K_F	n	R^2
As(V)	0.054	54.48	0.9965	6.751	2.080	0.9773
Pb(II)	0.022	65.79	0.9977	3.688	1.774	0.9927
Ni(II)	0.078	76.34	0.9992	9.332	1.886	0.9868

adsorption onto the Fe_3O_4/rGO were calculated by plotting of q_e versus C_e and the results are presented in Table 4. The equilibrium data of metal ion adsorption onto the Fe_3O_4/rGO can be well fitted by the two adsorption isotherm models since the coefficients of determination (R^2) in the two models are very close. The high correlation to both Langmuir and Freundlich isotherms implies a monolayer adsorption and the existence of heterogeneous surface in the adsorbents, respectively. This observation is similar to the paper reported by Kong et al. [43], in which both Langmuir and Freundlich models were well fitted to describe the adsorption of As(V) on nanoscale Fe-Mn binary oxides loaded on zeolite. The maximum adsorption amounts of As(V), Pb(II), and Ni(II) over Fe_3O_4/rGO calculated by Langmuir model are 58.48 mg/g for As(V), 65.79 mg/g for Pb(II), and 76.34 mg/g for Ni(II), rather higher than the other reports [43–46]. This result demonstrates that the obtained Fe_3O_4/rGO nanocomposite is a potential adsorbent for treating water sources contaminated by heavy metals.

4. Conclusion

Fe_3O_4/rGO nanocomposite was synthesized by a facile one-step process. The iron oxide in magnetic iron oxide is highly dispersed over rGO. The morphology of Fe_3O_4/rGO consists of very fine spherical particles in nanoscales. Fe_3O_4/rGO exhibits superparamagnetic properties at room temperature and saturation magnetization approaching 59 emu g^{-1}. The adsorption of As(V), Ni(II), and Pb(II) on the Fe_3O_4/rGO was fitted well to the *pseudo*-second-order kinetic model and obeyed both Langmuir and Freundlich models, which indicates surface heterogeneity and monolayer adsorption of the adsorbents. The Fe_3O_4/rGO exhibits excellent heavy metals adsorption. The maximum monolayer adsorption capacities calculated by Langmuir equation are 58.48 mg/g for As(V), 65.79 mg/g for Pb(II), and 76.34 mg/g for Ni(II). The Fe_3O_4/rGO nanocomposite can be used as a potential absorbent for removing toxic ion metals from aqueous solution.

Competing Interests

The authors declare that they have no competing interests.

Acknowledgments

This work was funded by the project of Vietnamese Ministry of Education and Training (no. B2014-28-39).

References

[1] H. I. Adegoke, F. A. Adekola, O. S. Fatoki, and B. J. Ximba, "Sorptive interaction of oxyanions with iron oxides: a Review," *Polish Journal of Environmental Studies*, vol. 22, no. 1, pp. 7–24, 2013.

[2] S. Klas and D. W. Kirk, "Advantages of low pH and limited oxygenation in arsenite removal from water by zero-valent iron," *Journal of Hazardous Materials*, vol. 252-253, pp. 77–82, 2013.

[3] P. L. Smedley and D. G. Kinniburgh, "A review of the source, behaviour and distribution of arsenic in natural waters," *Applied Geochemistry*, vol. 17, no. 5, pp. 517–568, 2002.

[4] V. Coman, B. Robotin, and P. Ilea, "Nickel recovery/removal from industrial wastes: a review," *Resources, Conservation and Recycling*, vol. 73, pp. 229–238, 2013.

[5] F. S. Hoseinian, M. Irannajad, and A. J. Nooshabadi, "Ion flotation for removal of Ni(II) and Zn(II) ions from wastewaters," *International Journal of Mineral Processing*, vol. 143, pp. 131–137, 2015.

[6] P. K. Pandey, S. K. Sharma, and S. S. Sambi, "Removal of lead (II) from waste water on zeolite-NaX," *Journal of Environmental Chemical Engineering*, vol. 3, no. 4, pp. 2604–2610, 2015.

[7] C. M. Zvinowanda, J. O. Okonkwo, P. N. Shabalala, and N. M. Agyei, "A novel adsorbent for heavy metal remediation in aqueous environments," *International Journal of Environmental Science and Technology*, vol. 6, no. 3, pp. 425–434, 2009.

[8] D. Mohan and C. U. Pittman Jr., "Arsenic removal from water/wastewater using adsorbents—a critical review," *Journal of Hazardous Materials*, vol. 142, no. 1-2, pp. 1–53, 2007.

[9] A. K. Geim and K. S. Novoselov, "The rise of graphene," *Nature Materials*, vol. 6, no. 3, pp. 183–191, 2007.

[10] R. F. Service, "Carbon sheets an atom thick give rise to graphene dreams," *Science*, vol. 324, no. 5929, pp. 875–877, 2009.

[11] Y.-B. Luo, J.-S. Cheng, Q. Ma, Y.-Q. Feng, and J.-H. Li, "Graphene-polymer composite: extraction of polycyclic aromatic hydrocarbons from water samples by stir rod sorptive extraction," *Analytical Methods*, vol. 3, no. 1, pp. 92–98, 2011.

[12] J. Chen, J. Zou, J. Zeng et al., "Preparation and evaluation of graphene-coated solid-phase microextraction fiber," *Analytica Chimica Acta*, vol. 678, no. 1, pp. 44–49, 2010.

[13] R. D. Ambashta and M. Sillanpää, "Water purification using magnetic assistance: a review," *Journal of Hazardous Materials*, vol. 180, no. 1–3, pp. 38–49, 2010.

[14] X. G. Luo and L. N. Zhang, "High effective adsorption of organic dyes on magnetic cellulose beads entrapping activated carbon," *Journal of Hazardous Materials*, vol. 171, no. 1–3, pp. 340–347, 2009.

[15] F. A. He, J. T. Fan, D. Ma, L. M. Zhang, C. Leung, and H. L. Chan, "The attachment of Fe_3O_4 nanoparticles to graphene oxide by covalent bonding," *Carbon*, vol. 48, no. 11, pp. 3139–3144, 2010.

[16] Y.-B. Luo, Z.-G. Shi, Q. Gao, and Y.-Q. Feng, "Magnetic retrieval of graphene: extraction of sulfonamide antibiotics from environmental water samples," *Journal of Chromatography A*, vol. 1218, no. 10, pp. 1353–1358, 2011.

[17] T. Qi, C. Huang, S. Yan, X.-J. Li, and S.-Y. Pan, "Synthesis, characterization and adsorption properties of magnetite/reduced graphene oxide nanocomposites," *Talanta*, vol. 144, pp. 1116–1124, 2015.

[18] L. Feng, M. Cao, X. Ma, Y. Zhu, and C. Hu, "Superparamagnetic high-surface-area Fe_3O_4 nanoparticles as adsorbents for arsenic removal," *Journal of Hazardous Materials*, vol. 217-218, pp. 439–446, 2012.

[19] L. Guo, P. Ye, J. Wang, F. Fu, and Z. Wu, "Three-dimensional Fe_3O_4-graphene macroscopic composites for arsenic and arsenate removal," *Journal of Hazardous Materials*, vol. 298, pp. 28–35, 2015.

[20] X. Guo, B. Du, Q. Wei et al., "Synthesis of amino functionalized magnetic graphenes composite material and its application to remove Cr(VI), Pb(II), Hg(II), Cd(II) and Ni(II) from contaminated water," *Journal of Hazardous Materials*, vol. 278, pp. 211–220, 2014.

[21] W. Zhang, X. Shi, Y. Zhang, W. Gu, B. Li, and Y. Xian, "Synthesis of water-soluble magnetic graphene nanocomposites for recyclable removal of heavy metal ions," *Journal of Materials Chemistry A*, vol. 1, no. 5, pp. 1745–1753, 2013.

[22] H. Ravishankar, J. Wang, L. Shu, and V. Jegatheesan, "Removal of Pb (II) ions using polymer based graphene oxide magnetic nano-sorbent," *Process Safety and Environmental Protection*, 2016.

[23] N. Danesh, M. Hosseini, M. Ghorbani, and A. Marjani, "Fabrication, characterization and physical properties of a novel magnetite graphene oxide/Lauric acid nanoparticles modified by ethylenediaminetetraacetic acid and its applications as an adsorbent for the removal of Pb(II) ions," *Synthetic Metals*, vol. 220, pp. 508–523, 2016.

[24] W. S. Hummers Jr. and R. E. Offeman, "Preparation of graphitic oxide," *Journal of the American Chemical Society*, vol. 80, no. 6, p. 1339, 1958.

[25] P. Zong, S. Wang, Y. Zhao, H. Wang, H. Pan, and C. He, "Synthesis and application of magnetic graphene/iron oxides composite for the removal of U(VI) from aqueous solutions," *Chemical Engineering Journal*, vol. 220, pp. 45–52, 2013.

[26] C. Wang, C. Feng, Y. Gao, X. Ma, Q. Wu, and Z. Wang, "Preparation of a graphene-based magnetic nanocomposite for the removal of an organic dye from aqueous solution," *Chemical Engineering Journal*, vol. 173, no. 1, pp. 92–97, 2011.

[27] A. Kumar, B. Prasad, and I. M. Mishra, "Adsorptive removal of acrylonitrile by commercial grade activated carbon: kinetics, equilibrium and thermodynamics," *Journal of Hazardous Materials*, vol. 152, no. 2, pp. 589–600, 2008.

[28] P. S. Teo, H. N. Lim, N. M. Huang, C. H. Chia, and I. Harrison, "Room temperature *in situ* chemical synthesis of Fe_3O_4/graphene," *Ceramics International*, vol. 38, no. 8, pp. 6411–6416, 2012.

[29] M. Zhang and M. Jia, "High rate capability and long cycle stability Fe_3O_4-graphene nanocomposite as anode material for lithium ion batteries," *Journal of Alloys and Compounds*, vol. 551, pp. 53–60, 2013.

[30] Y.-P. Chang, C.-L. Ren, J.-C. Qu, and X.-G. Chen, "Preparation and characterization of Fe_3O_4/graphene nanocomposite and investigation of its adsorption performance for aniline and *p*-chloroaniline," *Applied Surface Science*, vol. 261, pp. 504–509, 2012.

[31] D. Yang, X. Wang, J. Shi et al., "*In situ* synthesized rGO-Fe_3O_4 nanocomposites as enzyme immobilization support for achieving high activity recovery and easy recycling," *Biochemical Engineering Journal*, vol. 105, pp. 273–280, 2016.

[32] M. Z. Kassaee, E. Motamedi, and M. Majdi, "Magnetic Fe_3O_4-graphene oxide/polystyrene: fabrication and characterization of a promising nanocomposite," *Chemical Engineering Journal*, vol. 172, no. 1, pp. 540–549, 2011.

[33] L. T. Lanh, T. T. Hoa, N. D. Cuong et al., "Shape and size controlled synthesis of Au nanorods: H_2S gas-sensing characterizations and antibacterial application," *Journal of Alloys and Compounds*, vol. 635, pp. 265–271, 2015.

[34] N. A. Khan, Z. Hasan, and S. H. Jhung, "Adsorptive removal of hazardous materials using metal-organic frameworks (MOFs): a review," *Journal of Hazardous Materials*, vol. 244-245, pp. 444–456, 2013.

[35] L.-C. Shen, X.-T. Nguyen, and N. P. Hankins, "Removal of heavy metal ions from dilute aqueous solutions by polymer–surfactant aggregates: a novel effluent treatment process," *Separation and Purification Technology*, vol. 152, pp. 101–107, 2015.

[36] Y. Mamindy-Pajany, C. Hurel, N. Marmier, and M. Roméo, "Arsenic adsorption onto hematite and goethite," *Comptes Rendus Chimie*, vol. 12, no. 8, pp. 876–881, 2009.

[37] N. Mohammadi, H. Khani, V. K. Gupta, E. Amereh, and S. Agarwal, "Adsorption process of methyl orange dye onto mesoporous carbon material-kinetic and thermodynamic studies," *Journal of Colloid and Interface Science*, vol. 362, no. 2, pp. 457–462, 2011.

[38] V. Vadivelan and K. V. Kumar, "Equilibrium, kinetics, mechanism, and process design for the sorption of methylene blue onto rice husk," *Journal of Colloid and Interface Science*, vol. 286, no. 1, pp. 90–100, 2005.

[39] K. Periasamy and C. Namasivayam, "Process development for removal and recovery of cadmium from waste water by a low-cost adsorbent: adsorption rates and equilibrium studies," *Industrial and Engineering Chemistry Research*, vol. 33, no. 2, pp. 317–320, 1994.

[40] Y. S. Ho and G. S. McKay, "The kinetics of sorption of divalent metal ions onto sphagnum moss peat," *Water Research*, vol. 34, no. 3, pp. 735–742, 2000.

[41] S. C. Ma, J. L. Zhang, D. H. Sun, and G. X. Liu, "Surface complexation modeling calculation of Pb(II) adsorption onto

the calcined diatomite," *Applied Surface Science*, vol. 359, pp. 48–54, 2015.

[42] G. Sheng, Y. Li, X. Yang et al., "Efficient removal of arsenate by versatile magnetic graphene oxide composites," *RSC Advances*, vol. 2, no. 32, pp. 12400–12407, 2012.

[43] S. Kong, Y. Wang, H. Zhan, S. Yuan, M. Yu, and M. Liu, "Adsorption/oxidation of arsenic in groundwater by nanoscale fe-mn binary oxides loaded on zeolite," *Water Environment Research*, vol. 86, no. 2, pp. 147–155, 2014.

[44] X.-Q. Sun, B. Peng, Y. Ji, J. Chen, and D. Li, "Chitosan(chitin)/cellulose composite biosorbents prepared using ionic liquid for heavy metal ions adsorption," *AIChE Journal*, vol. 55, no. 8, pp. 2062–2069, 2009.

[45] M.-W. Wan, C.-C. Kan, B. D. Rogel, and M. L. P. Dalida, "Adsorption of copper (II) and lead (II) ions from aqueous solution on chitosan-coated sand," *Carbohydrate Polymers*, vol. 80, no. 3, pp. 891–899, 2010.

[46] P. Suresh Kumar, R. Q. Flores, C. Sjöstedt, and L. Önnby, "Arsenic adsorption by iron-aluminium hydroxide coated onto macroporous supports: insights from X-ray absorption spectroscopy and comparison with granular ferric hydroxides," *Journal of Hazardous Materials*, vol. 302, pp. 166–174, 2016.